Supporting information

Electrical detection of plasmon-induced isomerization in molecule-nanoparticle network devices

Didier Stiévenard,[1] David Guérin,[1] Stéphane Lenfant,[1] Gaëtan Lévêque,[1] Christian A. Nijhuis[2,3,4] & DominiqueVuillaume[1]*.

1) Institut d'Electronique, Microélectronique et Nanotechnologie (IEMN), CNRS, Université de Lille, Avenue Poincaré, F-59652cedex, Villeneuve d'Ascq, France.

2) Department of Chemistry, National University of Singapore, 3 Science Drive 3, 117543 Singapore, Singapore.

3) Centre for Advanced 2D Materials and Graphene Research Centre, National University of Singapore, 6 Science Drive 2, 117546 Singapore, Singapore.

4) NUSNNI-Nanocore, National University of Singapore, Singapore 117411, Singapore.

* corresponding author : dominique.vuillaume@iemn.fr

1. 2D-NPSAN : corrected current

For 2D NPSANs, it was not possible to obtain a stable current during the pre-configuration, the dark period and the LSP excitation. Figure S1 shows a typical current vs. time recorded for a sequence : pre-configuration in *trans* (470 nm light), dark, LSP excitation (590 nm) and dark. To extract the corrected current during PII shown in Fig. 3-a (main text), we subtracted a liner fit (blue line) from the raw data. Figure S2 shows the data when the AzBT are pre-configured in their *cis* state, and the fitted base line used to calculate the corrected current shown in Fig. 3-b.

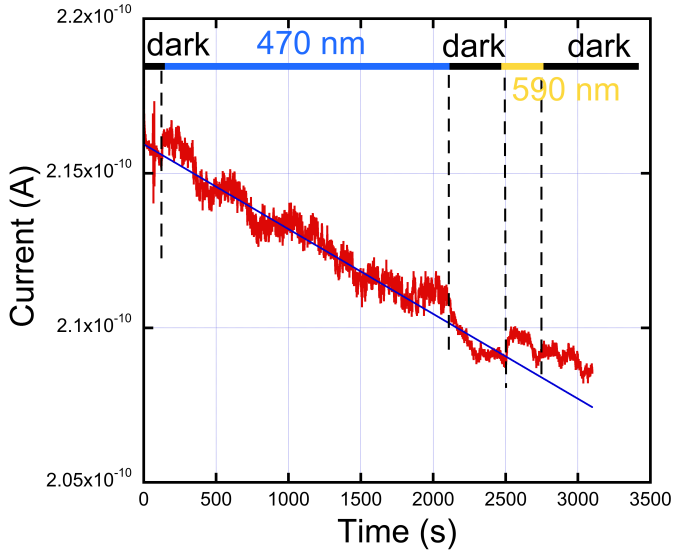

Figure S1. *Measured current for the 2D NSPSAN under a sequence : pre-configuration in trans (470 nm light), dark, LSP excitation (590 nm) and dark. The blue line is a linear function : i = 2.16x10^{-10} - 2.74x10^{-15} t, fitted for 0<t<2500 and extrapolated to subtract the base line in Fig. 3-a.*

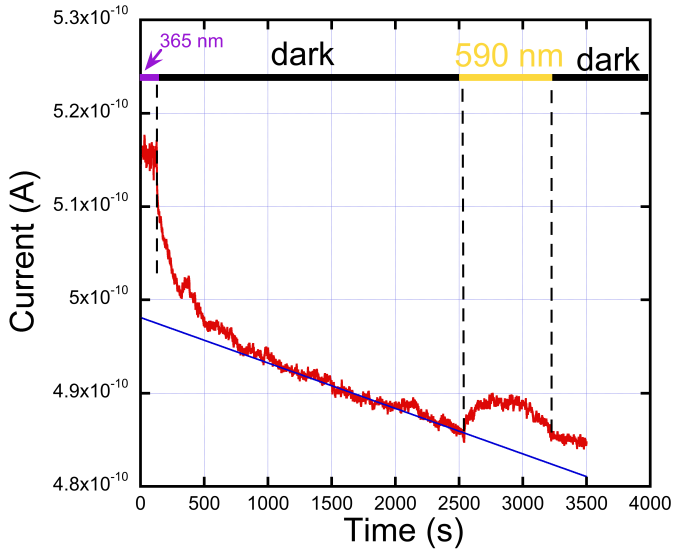

Figure S2. *Measured current for the 2D NSPSAN under a sequence : pre-configuration in cis (365 nm light), dark, LSP excitation (590 nm) and dark. The blue line is a linear function : i = 4.98x10^{-10} - 4.87x10^{-15} t, fitted for 1000<t<2500 and extrapolated to subtract the base line in Fig. 3-b.*

2. UV-vis isomerization.

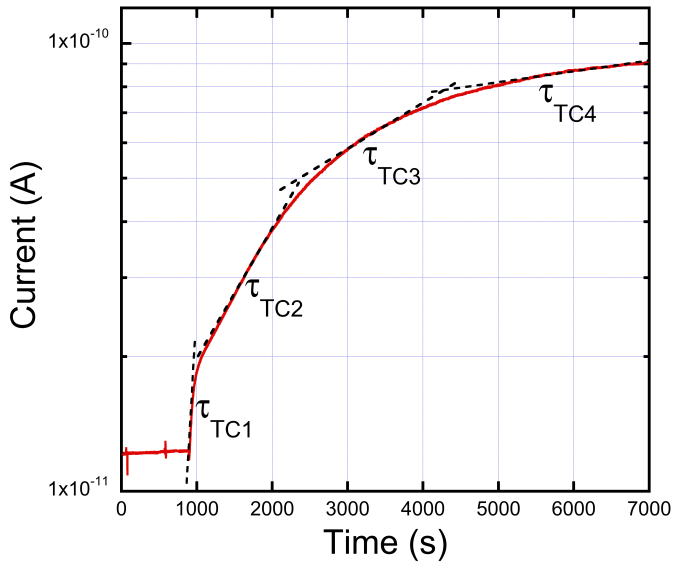

Figure S3. *Semilog plot of the trans to cis isomerization for the 2D-NPSANs (data form Fig. 4-a). We can extract several time constants :* τ_{TC1} *= 100 s,* τ_{TC2} *= 1360,* τ_{TC3} *= 1650 and* τ_{TC4} *= 2.2x10⁴ s*

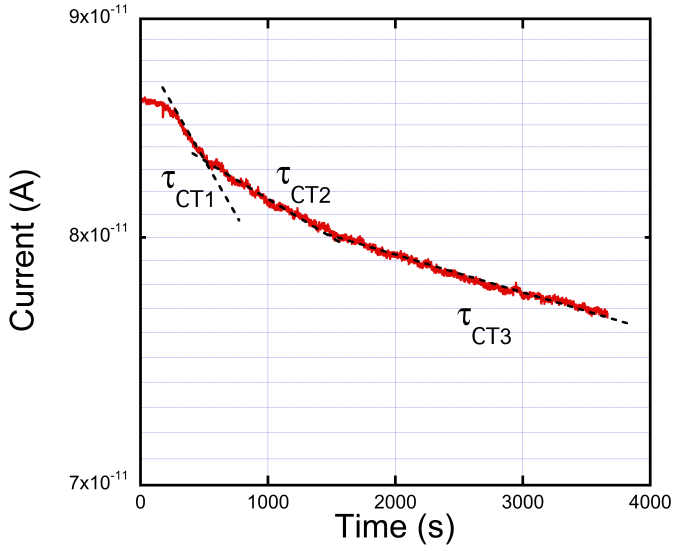

Figure S4. *Semilog plot of the cis to trans isomerization for the 2D-NPSANs (data form Fig. 4-b). We can extract several time constants :* τ_{CT1} *= 8900 s,* τ_{CT2} *= 3x10⁴ s and* τ_{CT3} *= 5.4x10⁴ s.*

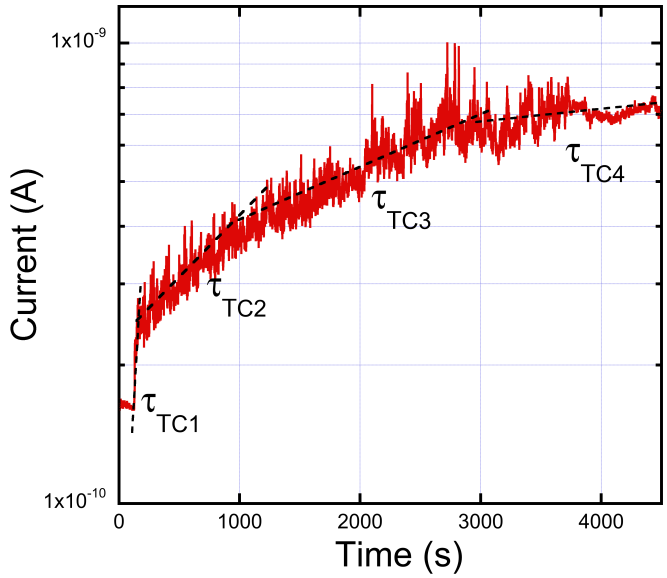

Figure S5. *Semilog plot of the trans to cis isomerization for the cluster-NPSANs (data form Fig. 4-c). We can extract several time constants :* τ_{TC1} *= 30 s,* τ_{TC2} *= 1570* τ_{TC3} *= 2900 and* $\tau_{TC4} = 1.35x10^4$ *s.*

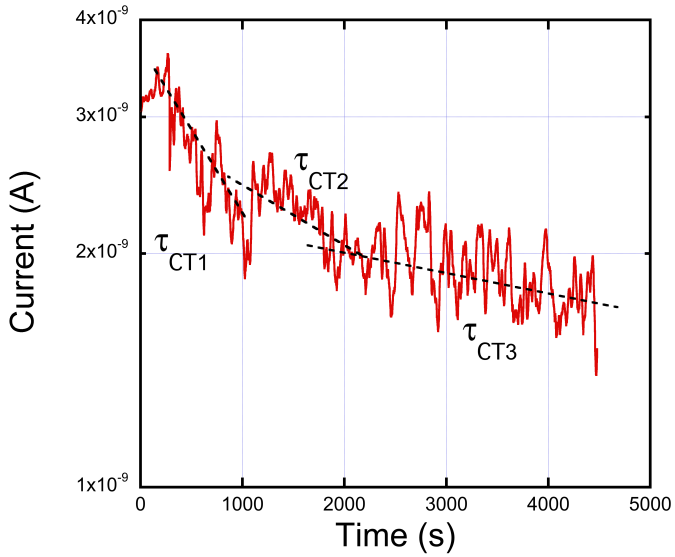

Figure S6. *Semilog plot of the cis to trans isomerization for the cluster-NPSANs (data form Fig. 4-d). We can extract several time constants :* τ_{CT1} *= 1950 s,* τ_{CT2} *= 4200 and* $\tau_{CT3} = 1.2x10^4$ *s.*

For the 2D-NPSANs, the *trans* to *cis* isomerization reveals several features, starting by a "fast" kinetics with a time constant of the order of τ_{TC1} = 100 s, followed by slower kinetics characterized by multi-exponential behaviors with time constants larger than ~10^3 s (Fig. S3). For the *cis* to *trans* isomerisation (Fig. S4) three typical time constants are extracted, with a first time constant τ_{CT1} = 8900 s much slower than for the *trans* to *cis* case. The same behavior is observed for the cluster-NSANs (Figs. S5 and S6). In the cluster-NPSANs the current levels are higher (as expected due to a more important number of current pathways), again with several time constants. The extracted time constants for the *trans*-to-*cis* isomerisation are of the order of τ_{TC1} = 30 s (Fig. S5), again followed by several time constants > 10^3 s. For the *cis* to *trans* isomerization, we have τ_{CT1} = 1950 s (Figure S6) for the first time constant. We note that these multi-exponential behaviors of the isomerization kinetics are quite similar for the 2D- and cluster-NPSANs, suggesting that the NP organizations are similar in the two types of devices, or that NP organization is of little importance to influence the AzBT isomerization. Table 1 summarizes all the measured time constants. We note that the multi-exponential behaviors of the UV-vis isomerization of AzBT in NPSANs differ from the previously observed behavior (single time constant) of the same molecules in a self-assembled monolayer, albeit an initial faster kinetics with a small amplitude is also observed for AzBT in SAMs.[1] This feature is likely related to a more disordered molecular structure in NPSANs.

	590 nm		365 nm *trans* to *cis*		470 nm *cis* to *trans*
	trans state (s)	*cis* state (s)	τ_{TC1} (s)	τ_{TCi} (s), i≥2	τ_{CTi} (s), i≥1
2D-NPSAN	22/63	n.a.	100	1360, 1650, $2.2x10^4$	8900, $3x10^4$, $5.4x10^4$
cluster-NPSAN	90	103	30	1570, 2900, $1.35x10^4$	1950, 4200, $1.2x10^4$

Table 1. Summary of the typical measured time constants under the 590 nm light irradiation for the cluster-NPSANs with the AzBT molecules in the *trans* state and *cis* state (Figs. 2-a and 2-b); similar data from Figs. 3-a and 3-b for the 2D-NPSANs with the AzBT molecules in the *trans* state only (see main text); and for both the 2D-NPSANs and cluster-NPSANs (data from Figs. 4 and S3-S6) under a 365 nm light irradiation (*trans* to *cis* isomerisation) and 470 nm light irradiation (*cis* to *trans* isomerisation).

3. PAT current.

The PAT current is calculated from the amplification factor M of the local electric field induced by the LSP between NPs for various NP sizes (10-60 nm) and gap distance between adjacent NPs (1-5 nm). These simulations show (next section 4, Fig. S8) that M does not overcome a value of ~10 for NPs with a diameter of 10 nm, spaced by an average gap of 4.5 nm and up to ca. 80 for a gap of around 1 nm. With a light power of 11.5 mW at 590 nm, the incident electric field E_0 is ~ $2.9x10^{-2}$ V/cm, as calculated from $P=0.5(\varepsilon/\mu)^{0.5}E^2$ with P the light power, ε and μ the permittivity and permeability in vacuum. Thus, we estimated $E_\omega = ME_0 = 2.9x10^{-1}$ V/cm. Therefore, as the nano-gap between two NP is ~ 4.5 nm,[2] the average LSP electric field V_ω across the NP-molecule-NP gap is of the order of $1.3x10^{-7}$ V. We calculated an upper limit of the PAT-induced change in the molecular conductance $\Delta G_{mol} = G_{dc}(\omega) - G_{dc}(0) = 8.25x10^{-20}$ S using Eq. (1) in the main text, considering that the transmission coefficient though the molecule τ(EF

± ħω) is 1 at the maximum. We converted ΔG_{mol} to ΔI, the PAT-induced current in the NPSAN, according to the following approach. Taking into account that about 200 molecules are inserted in the nanogap between two adjacent NPs (see Molecular Dynamics calculations in Ref. 2), we have $\Delta G_J = 200\Delta G_{mol}$ with ΔG_J the conductance of one NP-molecules-NP junction. Assuming a hexagonal compact organization of the NPs in the network, the sheet conductance in the NPSAN is $\Delta G_{\square} = (2/\sqrt{3})\Delta G_J$, with $\Delta G_{\square} = \Delta G^*L/W$; with the NPSAN conductance $\Delta G=\Delta I/V$ (V the dc applied voltage, 2.5 V), L (150 nm) the length between the electrodes and W (40 nm) the width (see Fig. 1-c). Thus, from $\Delta G_{mol} = 8.25\text{x}10^{-20}$ S, we estimated an upper limit for the PAT-induced current $\Delta I = 1.3\text{x}10^{-17}$ A.

4. UV-vis spectrum

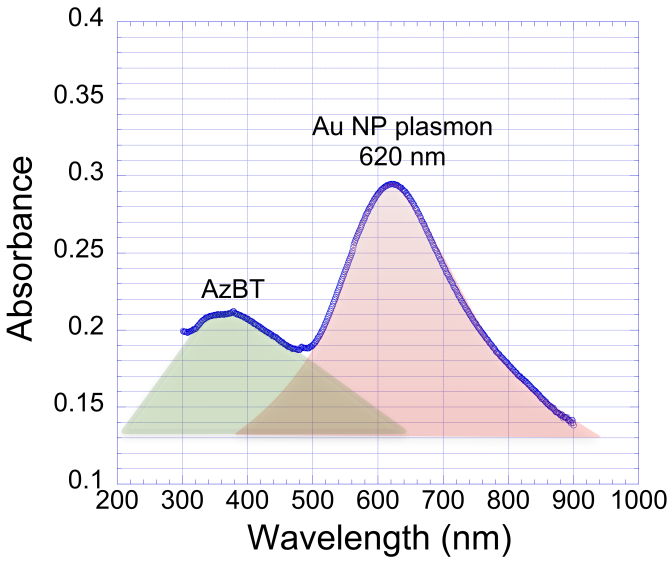

Figure S7. *UV-vis absorbance measurement for the trans-AzBT NPSAN deposited on quartz following the same methods as for NSPANs deposited on SiO_2 substrate used for electrical measurements (see Methods in the main paper). A transparent*

substrate is required for this measurement. Green and red areas are guides for eyes to highlight the contribution of the Au nanoparticules (LSP) and the AzBT (centered at 350-360 nm, see absorption of the AzBT molecules in Refs. 1, 3).

5. LSP simulations

Optical numerical simulations have been performed with a commercial finite element software (Comsol) on a modeled cluster-NPSAN. It consists in gold nanoparticles with 10nm diameter packed in a three-layer closed-packed structure of FCC type, with interparticle separation fixed to 4.5 nm. The cluster-NPSAN lies on a silica substrate, and is illuminated by a plane wave in oblique incidence (45°) from air. Transmission is computed in silica. The dielectric constant of gold is from Johnson and Christy,[4] and size correction has been applied as the diameter of the nanospheres is comparable to the mean free path of the conduction electron in gold.[5] The inter-particle medium is modeled as homogeneous and isotropic, and its dielectric constant has been adjusted in order to match the resonance wavelength of 630 nm obtained in UV-vis measurements (Fig. S7), which led to a value of 3.8, in agreement with literature for organic materials based on azobenzene derivatives.[6] The obtained M-factor is about 6.5 at resonance.

Then, we have estimated numerically the M-factor as a function of the gap and radius in a dimer of gold nanospheres embedded in an homogeneous medium of dielectric constant 3.8, at a fixed wavelength of 590 nm corresponding to the experimental LSP excitation. Simulations were done using a multi-particle Mie method.[7] The enhancement factor M reaches about 80 for a gap of 1 nm and radius of 15 nm, and drops to 11 for a gap of 4.5 nm and radius 5nm in our case (red cross). This value is slightly larger than in the modeled NPSAN due to increased confinement of light within the dimer.

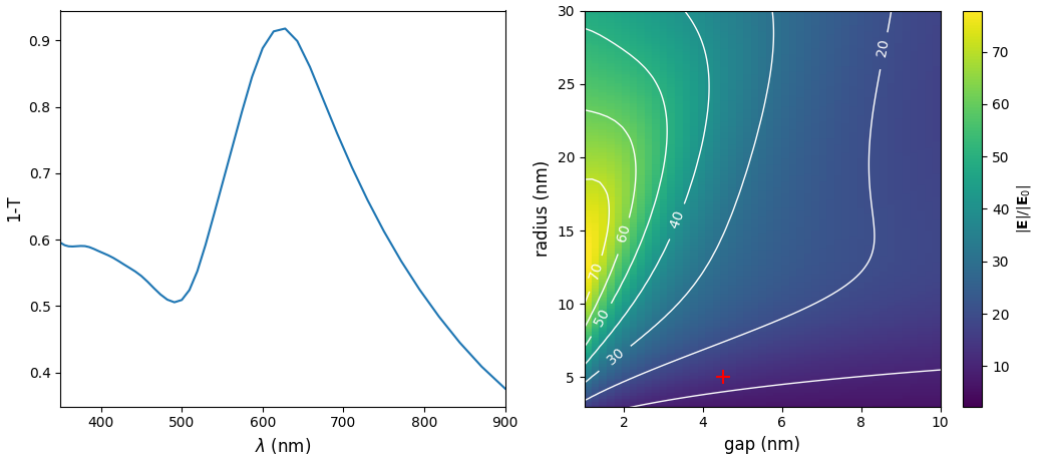

***Figure S8**: (a) Extinction spectrum of the modeled three-layer cluster-NSPAN, with a dielectric constant of 3.8 for the interparticle medium. (b) M-factor as a function of gap and radius of two gold nanospheres in a homogeneous medium with refractive index 3.8. The field is computed 0.2nm away from one nanosphere surface, inside the gap. The red cross marks a radius of 5 nm and gap 4.5 nm.*

6. Electrical switching of AzBT

In STM studies reported in Ref. 8, the molecules are lying flat on Au(111) surface, and the samples are in UHV and at 5K. Such configuration and conditions are quite different from our case. Moreover, during the STM measurements, the electric field is applied perpendicular to the surface/molecule whereas in our case, various angles exist between the plasmonic electric field and the molecules covering the Au NPs. This is of prime importance because the orientation of the molecule (i.e. its permanent dipole and the component of its polarizability tensor along the electric field direction) is a key factor for the isomerization.[9] We also note that for Au(100) or Cu(111) surfaces,[10] no switching effect was detected, showing that these observations are surface dependent, and, to the best of our

knowledge, electrical switching of azobenzene has only been reported in Ref. 8. Finally, STM experiments used a static electric field compared to a dynamic one in our case.

7. AFM images.

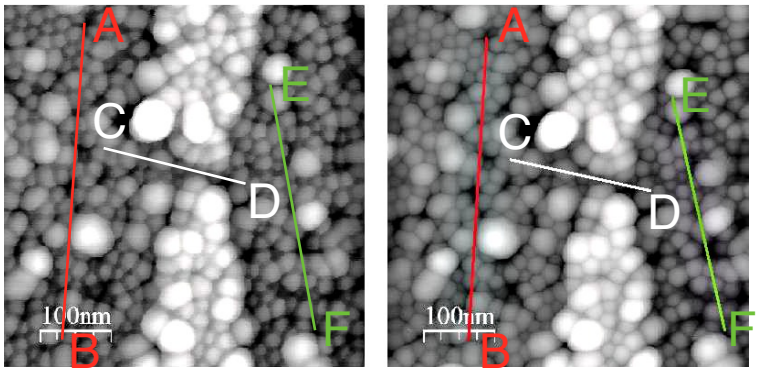

Figure S9. *AFM images of the NPSANs with the AzBT in the trans isomer (left) and cis isomer (right). We do not observed a significant modification of the NP network morphology. We only note some random distance variations, which may be due fluctuations during the long time of experiments (light illumination and AFM images). Formation example, the point-to-point distances AB (421 nm), CD (305 nm) and EF (337 nm) vary by -4.9%, -0.1% and +4.1%, between the trans and cis isomers, respectively. This ±5% relative variation applied to the inter-NP distance correspond to ±0.22 nm, i.e below the statistical size distribution of ± 1 nm.*[2]

References

1. Smaali, K.; Lenfant, S.; Karpe, S.; Oçafrain, M.; Blanchard, P.; Deresmes, D.; Godey, S.; Rochefort, A.; Roncali, J.; Vuillaume, D. *ACS Nano* **2010,** 4, (4), 2411-2421.

2. Viero, Y.; Copie, G.; Guerin, D.; Krzeminski, C.; Vuillaume, D.; Lenfant, S.; Cleri, F. *J. Phys. Chem. C* **2015,** 119, 21173-21183.

3. Karpe, S.; Ocafrain, M.; Smaali, K.; Lenfant, S.; Vuillaume, D.; Blanchard, P.; Roncali, J. *Chemical Communications* **2010,** 46, (21), 3657-3659.

4. Johnson, P. B.; Christy, R. W. *Phys. rev. B* **1972,** 6, 4370.

5. Berciaud, S.; Cognet, L.; Tamarat, P.; Lounis, B. *Nano Lett* **2005,** 5, 515-518.

6. Stangenberg, R.; Grigoriadis, C.; Butt, H.-J.; Müllen, K.; Floudas, G. *Colloid and Polymer Science* **2014,** 292, (8), 1939-1948.

7. Xu, Y.-I.; Gustafson, B. Journal of Quantitative Spectroscopy & Radiative Transfer **2001,** 70, 395-419.

8. Alemani, M.; Peters, M. V.; Hecht, S.; Rieder, K.-H.; Moresco, F.; Grill, L. *J Am Chem Soc* **2006,** 128, (45), 14446-14447.

9. Füchsel, G.; Klamroth, T.; Dokić, J.; Saalfrank, P. *J Phys Chem B* **2006,** 110, (33), 16337-16345.

10. Alemani, M.; Selvanathan, S.; Ample, F.; Peters, M. V.; Rieder, K.-H.; Moresco, F.; Joachim, C.; Hecht, S.; Grill, L. *J. Phys. Chem. C* **2008,** 112, (28), 10509-10514.